

# Structure and Flexibility of *Streptococcus agalactiae* Hyaluronate Lyase Complex with Its Substrate

INSIGHTS INTO THE MECHANISM OF PROCESSIVE DEGRADATION OF HYALURONAN\*

Received for publication, May 24, 2002, and in revised form, July 16, 2002  
Published, JBC Papers in Press, July 18, 2002, DOI 10.1074/jbc.M205140200

Luciane V. Mello‡§, Bert L. de Groot¶, Songlin Li||, and Mark J. Jedrzejas‡||\*\*

From the ‡Children's Hospital Oakland Research Institute, Oakland, California 94609, §National Centre of Genetic Resources and Biotechnology, Cenargen/Embrapa, 70770-900 Brasília, Brazil, ¶Max Planck Institute for Biophysical Chemistry, 37077 Göttingen, Germany, and ||Department of Microbiology, University of Alabama at Birmingham, Birmingham, Alabama 35294

***Streptococcus agalactiae* hyaluronate lyase degrades primarily hyaluronan, the main polysaccharide component of the host connective tissues, into unsaturated disaccharide units as the end product. Such function of the enzyme destroys the normal connective tissue structure of the host and exposes the tissue cells to various bacterial toxins. The crystal structure of hexasaccharide hyaluronan complex with the *S. agalactiae* hyaluronate lyase was determined at 2.2 Å resolution; the mechanism of the catalytic process, including the identification of specific residues involved in the degradation of hyaluronan, was clearly identified. The enzyme is composed structurally and functionally from two distinct domains, an α-helical α-domain and a β-sheet β-domain. The flexibility of the protein was investigated by comparing the crystal structures of the *S. agalactiae* and the *Streptococcus pneumoniae* enzymes, and by using essential dynamics analyses of CONCOORD computer simulations. These revealed important modes of flexibility, which could be related to the protein function. First, a rotation/twist of the α-domain relative to the β-domain is potentially related to the mechanism of processivity of the enzyme; this twist motion likely facilitates shifting of the ligand along the catalytic site cleft in order to reposition it to be ready for further cleavage. Second, a movement of the α- and β-domains with respect to each other was found to contribute to a change in electrostatic characteristics of the enzyme and appears to facilitate binding of the negatively charged hyaluronan ligand. Third, an opening/closing of the substrate binding cleft brings a catalytic histidine closer to the cleavable substrate β1,4-glycosidic bond. This opening/closing mode also reflects the main conformational difference between the crystal structures of the *S. agalactiae* and the *S. pneumoniae* hyaluronate lyases.**

*Streptococcus agalactiae* is a human pathogenic bacterium, which is one of the major causes of meningitis and septicemia, especially for neonates and pregnant women. *S. agalactiae*, similarly to other Gram-positive pathogens, produces a variety of virulence factors, some of which are exposed on the surface of bacterial cell. In addition to the primary virulence factor of this organism, the polysaccharide capsule, there are several known surface-accessible proteins expressed by the bacterium that significantly contribute to the total virulence of this organism. An example of such a surface-exposed protein virulence factor of *S. agalactiae* is hyaluronate lyase. The primary function of this enzyme is the degradation of hyaluronan (HA),<sup>1</sup> the predominant polysaccharide component of animal connective tissues and nervous system. The final hyaluronan degradation product by the enzyme is the unsaturated disaccharide unit of HA, 2-acetamido-2-deoxy-3-O-(β-D-glucosyluronic acid)-D-glucose (ΔDi-HA) (1). The *S. agalactiae* bacterial strains that produce more extracellular hyaluronate lyase were shown to be more virulent than those strains producing less of this enzyme, although these strains are usually asymptomatic in humans (2, 3). This property together with additional studies suggests that hyaluronate lyase action may account for the major part of the mortality and morbidity associated with the *S. agalactiae* infection in humans.

Hyaluronan, the main substrate for hyaluronate lyase, is composed of linear polymeric repeats of a few hundred to a few thousand disaccharide units of hyaluronic acid, D-glucuronic acid(1-β-3)N-acetyl-D-glucosamine(1-β-4). HA is detectable in every studied tissue and fluid in higher animals and in humans (4). It forms a strikingly viscoelastic matrix, which in part serves as a medium for connective tissue cells. *In vivo* degradation and metabolism of HA occur at high rates, often higher than those for other polysaccharides. The HA degradation and metabolism is highly active as compared with degradation and metabolism of other polysaccharides *in vivo*. In humans, approximately one-third of the total hyaluronan (about 5 g) is turned over on a daily basis (5). Such a rapid turnover rate was found to facilitate the role of HA and its degradation products in many physiological processes such as cell differentiation and embryo development (6), cell proliferation, recognition, locomotion, tumor development, and the immunological responses (4).

\* This work was supported by National Institutes of Health Grant AI 44079 (to M. J. J.). The costs of publication of this article were defrayed in part by the payment of page charges. This article must therefore be hereby marked "advertisement" in accordance with 18 U.S.C. Section 1734 solely to indicate this fact.

The atomic coordinates and structure factors (code 1LXM) have been deposited in the Protein Data Bank, Research Collaboratory for Structural Bioinformatics, Rutgers University, New Brunswick, NJ (<http://www.rcsb.org/>).

\*\* To whom correspondence should be addressed: Children's Hospital Oakland Research Institute, 5700 Martin Luther King Jr. Way, Oakland, CA 94609. Tel.: 510-450-7932; Fax: 510-450-7910; E-mail: mjedrzejas@chori.org.

<sup>1</sup> The abbreviations used are: HA, hyaluronan; ED, essential dynamics; HA1, HA2, and HA3, consecutive positions of hyaluronan disaccharides within the hexasaccharide substrate numbered from the reducing toward the non-reducing end; KSCN, potassium thiocyanate; MD, molecular dynamics; NAc, N-acetyl-β-D-glucosamine; PDB, protein data bank; HL, hyaluronate lyase; GlcA, β-D-glucuronic acid; ΔDi-HA, 2-acetamido-2-deoxy-3-O-(β-D-glucosyluronic acid)-D-glucose.

Enzymes from either mammalian or bacterial origin degrade HA mainly at the  $\beta$ 1,4 linkages found between the disaccharide components of this polymer. Bacteria usually secrete hyaluronate lyases, which degrade HA by the  $\beta$ -elimination process and produce unsaturated di-, tetra-, or hexasaccharide units, whereas mammals express hyaluronidases, which degrade HA by the hydrolysis mechanism, and they produce relatively longer oligosaccharide units of HA of various sizes. The details of the mechanism of HA degradation by mammalian hyaluronidases are still largely unknown primarily because of the lack of structural information about these enzymes. Nevertheless, hyaluronidases of bovine origin, for example, are widely used in clinics as an additive to the local anesthesia for the faster spreading and penetration through tissues of selected medications (7, 8). It is likely that mammalian hyaluronidases, similar to other hydrolytic polysaccharide-degrading enzymes, utilize the direct or double displacement mechanism to degrade their substrate (9). Based on structural information, the mechanism of hyaluronan degradation by *Streptococcus* species hyaluronate lyase was recently proposed and was termed proton acceptance and donation (1, 10). This degradative process was shown to proceed through a processive mode of action (11) and to involve hyaluronan degradation in the direction from the reducing to the non-reducing end of the substrate (10).

The native structure of the *S. agalactiae* hyaluronate lyase and the structure of its complex with the disaccharide product of degradation,  $\Delta$ Di-HA, were recently elucidated by means of x-ray crystallography (10). The structures showed that the enzyme is built from three distinct domains. Starting from the N terminus these domains are as follows: a  $\beta$ -sheet  $\beta$ I-domain, an  $\alpha$ -helical  $\alpha$ -domain, and another  $\beta$ -sheet domain termed  $\beta$ II. The proton acceptance and donation mechanisms of action of this enzyme were proposed based on these structural data, the modeling studies of hyaluronan, the site-directed mutagenesis studies (12), and the comparison to *Streptococcus pneumoniae* hyaluronate lyase (1, 9, 13). The amino acid residues of the enzyme involved in this process were identified, and their specific roles and function in catalysis were suggested. Here we report a structure of the complex between the *S. agalactiae* hyaluronate lyase and the hexasaccharide unit of hyaluronan and the extensive computational analysis of the dynamic and flexibility properties of this enzyme. This information is then related to the mechanism of catalysis and the mechanism of processivity of hyaluronan degradation by bacterial hyaluronate lyases.

## EXPERIMENTAL PROCEDURES

**Production of the Enzyme and the Hexasaccharide Substrate, Crystallization of the Complex, and Collection of X-ray Diffraction Data**—The gene for *S. agalactiae* hyaluronate lyase (*hylB*<sub>3502</sub>, *hylB*<sub>4755</sub>) has been cloned and overexpressed in *Escherichia coli*. The enzyme was purified, and the crystallization sample was obtained as reported previously (14–16). The hexasaccharide substrate was obtained from human umbilical cord hyaluronan (Sigma) and purified also as described previously (1, 17). To prevent degradation the substrate was stored frozen at –80 °C in 10 mM Tris-HCl buffer, pH 8.0, until the time of use. The crystals of the native 92-kDa form of the *S. agalactiae* hyaluronate lyase were produced at room temperature as reported previously (10, 14), and the native crystals were used to obtain the complexes by soaking them with the hexasaccharide HA substrate also at room temperature using the hanging-drop vapor diffusion in 24-well Linbro culture plates. Briefly, the native crystals were soaked in 10–50 mM solution of hexasaccharide of hyaluronan in a 100 mM sodium cacodylate buffer, pH 6.0, 30 mM potassium thiocyanate (KSCN), and 30% polyethylene glycol monomethyl ether 5,000 for several days to several weeks.

Immediately before collecting diffraction data, the crystals of the complex were cryo-protected similarly to the procedures used for the native crystals (10, 14) by immersing them for a few seconds in the solution containing 22% glycerol, 30% polyethylene glycol monomethyl

ether 5,000, 30 mM KSCN, and 50 mM sodium cacodylate buffer at pH 6.0. The crystals were then frozen in a nitrogen flow at –170 °C using a Cryostream Cooler low temperature device (Cryosystems). Under such conditions, the crystals showed essentially no decay in the resolution of diffraction during diffraction data collection. The diffraction data sets were collected using synchrotron radiation at the wavelength of 1.0 Å at the 19-BM beamline at the Argonne National Laboratory, Advanced Photon Source, Structural Biology Center using an Oxford 3 × 3 CCD detector and/or at the Brookhaven National Laboratory, National Synchrotron Light Source, using beamline x25 and the Brandeis-4 CCD detector. The diffraction limit for these crystals was 2.20 Å. The diffraction data were processed and scaled using the HKL2000 package (18). The crystals of the hexasaccharide HA-hyaluronate lyase complex were isomorphous to the native crystals. The final parameters for the crystals and the diffraction data collected are reported in Table I.

**Three-dimensional Structure Determination of the Complex with Hyaluronan Hexasaccharide**—The three-dimensional native structure for *S. agalactiae* hyaluronate lyase (10) (Protein Data Bank (PDB) accession code 1F1S) was used as the initial model for the solution of the complex structure with the hexasaccharide hyaluronan. At first, a set of rigid body refinements was performed with the X-PLOR program (19) using the whole model as the starting point, followed by rigid body refinements of the individual domains of the molecule. The validation of the rigid body and all subsequent refinements was performed using the  $R_{\text{free}}$  methodology with 2.5% of all reflections (1,134 reflections) randomly selected for the validation data set (20). The progress of the refinements was inspected, and manual adjustments of the model were performed using the O program (21). The rigid body refinements were followed with the positional and simulated annealing refinement protocols of X-PLOR (19, 22). The structure was refined against the total of 45,372 reflections utilizing all data from 50.00 to 2.20 Å and a 2 $\sigma(F)$  cutoff (Table I). The following subsequent calculations of electron density allowed for clear identification of the substrate, which was then incorporated into this density. The topologies and parameter files for the substrate were created manually based on our earlier studies (10, 23, 24) and corrected to reflect the ideal stereochemistry. Additional refinements, including group and then individual restrained B-factor refinements, inspection, and manipulation of structure on graphics using the O program together with incorporation of water molecules placed into 3 $\sigma$  peaks in a  $\sigma$ -A weighted  $F_o - F_c$  map following standard criteria were performed. After additional refinements that followed, water molecules whose positions were not supported by electron density at the 1 $\sigma$  contouring level in  $\sigma$ -A weighted  $2F_o - F_c$  maps were deleted. A variety of stereochemical (25) and other analyses (21, 26) were periodically performed in order to locate possible errors in the structure. 191 water molecules were incorporated into the final structure of the complex. Final refinement statistics is provided in Table I.

**Flexibility Analyses**—In our earlier studies, the flexibility of another streptococcal hyaluronate lyase with known three-dimensional x-ray structure, from *S. pneumoniae*, was investigated and reported (23). In this study, we therefore performed a comparison between the flexibility of *S. agalactiae* hyaluronate lyase (*S. agalactiae* HL) (PDB code 1F1S) and *S. pneumoniae* hyaluronate lyase (*S. pneumoniae* HL) (PDB code 1EGU) using the DynDom program (27, 28). Given two sets of structures and protein coordinates, DynDom assigns rotation vectors for each amino acid residue, which together describe the transition from one conformation to the other. A clustering of the end points of these rotation vectors follows, and if consecutive stretches of residues with similar rotation vectors are found, these are termed dynamic domains. Because DynDom works on a residue basis, the structures of *S. agalactiae* HL and *S. pneumoniae* HL first had to be structurally aligned. For this, we first performed a sequence alignment using the WHAT\_IF program (29). The final aligned common part of both protein structures had a size of 716 amino acid residues. DynDom default parameters were used for the analysis, except for the minimal domain size that was set to 100.

**Structure Generation Using CONCOORD**—The CONCOORD program (30) generates mutually uncorrelated (protein) structures that fulfill a set of upper and lower interatomic distance limits, which are derived from experimental structures through calculation of interatomic distances and prediction of the interaction strength of the involved atoms. Although detailed aspects of dynamic variation are not reproduced by this method, good qualitative agreement has been found between results of conventional molecular dynamics (MD) and CONCOORD simulations, especially regarding large scale concerted protein fluctuations (30). CONCOORD is particularly suitable to be applied to large systems, where conventional molecular dynamics would require unfeasibly large amounts of computer time, and therefore it is finding

an increasing number of applications (31–33). A collection of conformations generated by CONCOORD can be thought of as a set of (uncorrelated) structural snapshots. Taken together, these conformations can in many ways be treated and analyzed in exactly the same way as, for example, a trajectory of snapshots produced by an MD simulation (30).

In our studies, 500 conformations were produced using CONCOORD for the hyaluronate lyase from *S. agalactiae*. Trajectories were generated for the *S. agalactiae* enzyme with (*S. agalactiae* HL) (domains included  $\beta$ I,  $\alpha$ , and  $\beta$ II) and without the most N-terminal part, the  $\beta$ I domain (*S. agalactiae* HL- $\beta$ I) (domains included  $\alpha$  and  $\beta$ II), and with and without the hexasaccharide ligand. A comparison of the structure with and without the  $\beta$ I domain was made in order to evaluate the influence of this domain on the overall protein flexibility.

**Essential Dynamics**—The essential dynamics (ED) method (34) is a powerful tool for filtering large scale concerted fluctuations from an ensemble of conformations, *e.g.* an MD trajectory (35) or a set of experimental structures (36). The method is equivalent to a principal component analysis and is based on the diagonalization of the covariance matrix of atomic fluctuations, which yields a set of eigen values and eigenvectors. The eigenvectors indicate directions in a  $3n$ -dimensional space (with  $n$  = the number of atoms of the protein) and describe concerted fluctuations of the atoms. The eigenvalues reflect the magnitude of the fluctuation along of the respective eigenvectors.

To compare ED properties of two simulations of similar systems, as for instance a wild type protein and its mutant, an ED analysis can be performed on a combined trajectory constructed by concatenating individual trajectories of these systems. Analysis of the behavior of the different parts of the trajectory provides a powerful tool for evaluating similarities and differences between the essential motions in different trajectories of a similar system. ED analyses were performed by Gromacs 3.0 (37, 38) for the two systems: *S. agalactiae* HL (all domains) and *S. agalactiae* HL- $\beta$ I (without the N-terminal  $\beta$ I domain).

Three combined analysis studies were carried out. In the first study, a combined trajectory was constructed by concatenating the two sets of 500 conformations produced by CONCOORD (here treated as trajectories) of the *S. agalactiae* enzyme with (*S. agalactiae* HL) and without the  $\beta$ I domain (*S. agalactiae* HL- $\beta$ I). For this analysis just the two domains, which are common to both structures, were included ( $\alpha$  and  $\beta$ II). A covariance matrix was built and diagonalized for the  $\alpha$ -carbon coordinates. The resulting eigenvectors were studied for possible dynamic differences.

In the second combined analysis the aim was to compare the dynamic properties of hyaluronate lyase from two related streptococcal species, *S. agalactiae* and *S. pneumoniae*, and to study possible differences in structure and dynamics between the two simulations. As a combined analysis can only be performed in systems that share the same size, a tertiary structure alignment between *S. pneumoniae* HL and *S. agalactiae* HL was performed using their crystal structures. A common core of the structure enzyme was formed using the parts of the protein which were present in both structures. This core represents  $\alpha$ -helices and  $\beta$ -sheets, which overlap between the two structures, and consists of 387 of 716 residues of the *S. agalactiae* enzyme. Thus, just the part of the trajectories generated by CONCOORD that correspond to this core protein was used for the combined essential dynamic analysis. For the *S. pneumoniae* hyaluronate lyase trajectories, we used the ones that we have previously generated for *S. pneumoniae* HL (23).

The third combined analysis was performed utilizing the trajectories of *S. agalactiae* HL, with and without the hexasaccharide substrate, to study the effect of the ligand onto the structure and flexibility of the protein.

**Other Methods**—The protein and hyaluronan substrate concentrations for the crystallization studies were determined as described previously (14). All figures were prepared using Ribbons (39), Grasp (40), O (21), or Molscript/Bobscript (41, 42) and Raster3D (43) programs.

## RESULTS AND DISCUSSION

### Structure Solution and Refinement

Previous modeling analysis of the streptococcal hyaluronate lyases (1, 10) suggested that the hexasaccharide hyaluronan substrate is the longest unit of hyaluronan that would completely fit within the catalytic cleft of the enzyme. Therefore, this substrate was chosen for structural studies. The hexasaccharide hyaluronan substrate was produced in milligram quantities from a human umbilical cord hyaluronan utilizing *Streptomyces hyalurolyticus* hyaluronate lyase degradation of polymeric hyaluronan as described under “Experimental Pro-

TABLE I  
X-ray diffraction data and structure refinement parameters for *S. agalactiae* hyaluronate lyase complex with the hexasaccharide unit of hyaluronan

Space group	C222 <sub>1</sub>
Unit cell dimensions (Å)	$a = 51.69, b = 157.03,$ $c = 239.20$
Resolution range (Å)	50.00–2.20
Measured reflections	233,927
Unique reflections	45,372
Completeness (last shell) <sup>a</sup> (%)	93.7 (71.4)
R <sub>merge</sub> <sup>b</sup> (last shell) (%)	14.4 (92.1)
Final model	795 out of 814 amino acids, 191 waters, 1 substrate molecule
R <sub>cryst</sub> <sup>c</sup> (last shell)	21.8 (32.6)
R <sub>free</sub> <sup>d</sup> (last shell)	27.1 (36.7)
Rmsd <sup>e</sup> bonds (Å)	0.008
Rmsd <sup>e</sup> angles	1.272
Average B-factors (Å <sup>2</sup> ) entire protein	35.10
$\beta$ I-domain	37.12
$\alpha$ -Domain	31.07
$\beta$ II-domain	38.87
Water molecules	49.07
Hexasaccharide substrate	98.10

<sup>a</sup> The last shell is defined as 2.20 to 2.28 Å.

<sup>b</sup> R<sub>merge</sub> =  $|I_i - \bar{I}|/I_i \times 100$  where  $I_i$  is the intensity of an individual reflection and  $\bar{I}$  is the mean of all reflections.

<sup>c</sup> /R<sub>cryst</sub> =  $\|F_p\| - \|F_{\text{calc}}\|/\|F_p\| \times 100$  where  $F_p$  and  $F_{\text{calc}}$  are the measured and the calculated structure factors, respectively.

<sup>d</sup> R<sub>free</sub> is as defined as in Brunger and Kruckowski (53).

<sup>e</sup> Rmsd, root mean square deviation.

cedures” and as reported previously (1, 17, 44, 53).

The crystallization of the native enzyme, crystal soaking with the hexasaccharide hyaluronan, x-ray diffraction data collection and processing, and structure solution and refinement were performed as described under “Experimental Procedures.” The data collected in Table I indicate a well refined structure with good stereochemistry. In a Ramachandran plot (25), the vast majority of the residues is located in the most favored areas, and none is in the disallowed region of the plot. The crystal structure was solved at 2.20 Å resolution (Fig. 1). The crystallized protein corresponds to residues Ala<sup>171</sup> to Ile<sup>984</sup> in the full-length enzyme (10, 14, 15). The structure of the current complex contains residues His<sup>173</sup> to Ile<sup>984</sup> that were visible in the electron density; two N-terminal residues and three groups of residues Phe<sup>714</sup>–Asp<sup>721</sup>, Asp<sup>813</sup>–Ser<sup>818</sup>, and Asn<sup>886</sup>–Asp<sup>889</sup> constituting three breaks in the structure, totaling up to 19 amino acid residues, were not observed in the electron density maps and therefore were not included in the final model of the structure. All three breaks in the observed electron density and in the structure are located in the surface loops, and the analysis of the electron density maps clearly suggests a disorder present in these parts of the structure. The electron density was clear for the remainder of the structure, including the hyaluronan substrate molecule (Fig. 1). The structure of the complex contains only 191 ordered water molecules that could be located during the final stages of refinement in addition to protein and the hexasaccharide hyaluronan substrate molecule. There was only one substrate molecule bound per molecule of the enzyme.

### Description of the Structures of the Enzyme and Hyaluronan

The structure of the enzyme in the current complex is very similar to the structure of the native protein (10). The enzyme, and its structure, is composed of three domains connected only by two short peptide linkers that are 7 and 11 amino acid residues long (Fig. 1A). These domains are from the N terminus

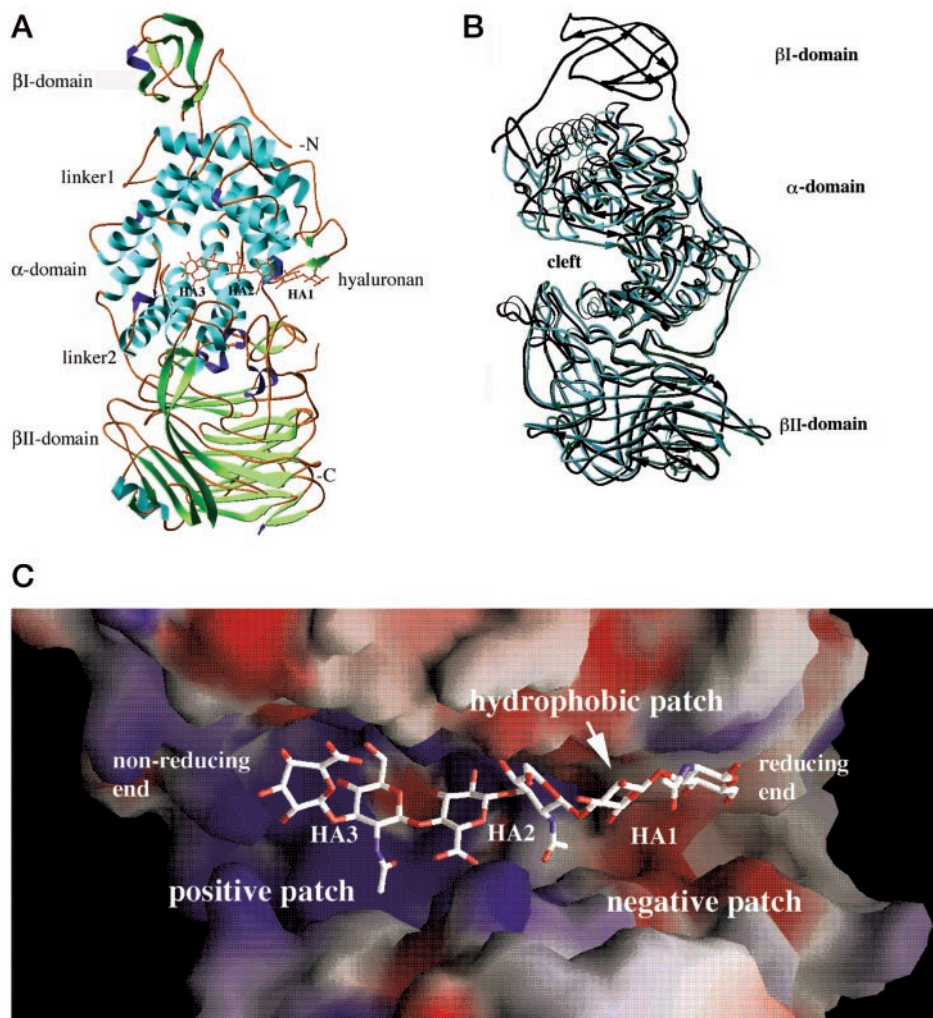


**FIG. 1. The structure of *S. agalactiae* hyaluronate lyase with bound hexasaccharide hyaluronan substrate.** *A*, ribbon drawing of the structure of the complex. All three domains of the enzyme are shown, the N-terminal  $\beta$ -sheet domain ( $\beta$ II-domain, top), the  $\alpha$ -helical domain ( $\alpha$ -domain, middle), the C-terminal  $\beta$ -sheet domain ( $\beta$ II-domain, bottom), as well as the cleft with the bound hexasaccharide unit of hyaluronan substrate (depicted in a ball and stick fashion with bonds colored in red). The structure of the enzyme is color-coded by the secondary structure elements ( $\alpha$ -helices in blue,  $3_{10}$  helices in purple,  $\beta$ -sheets in green), and the atoms of the substrate are colored by the atom type (carbon atoms in green, oxygen atoms in red, and nitrogen atoms in blue). Consecutive disaccharide units of HA starting from the reducing end are labeled as HA1, HA2, and HA3. *B*, comparison of structures of *S. agalactiae* and *S. pneumoniae* hyaluronate lyases. The *S. agalactiae* enzyme (black) (domains labeled) has an additional domain at its N terminus ( $\beta$ I-domain). The cleft area in this enzyme is also wider than that of the *S. pneumoniae* hyaluronate lyase (blue) (maximum difference in width of  $\sim 7$  Å). *C*, electrostatic potential distribution in the catalytic cleft. The positive potential is shown in blue and the negative potential in red. The majority of the cleft is highly positively charged (middle and the left side; positive patch) whereas at the product-releasing end of the cleft is negatively charged (right side of the cleft; a negative patch). The hydrophobic patch is also shown. Bound hexasaccharide hyaluronan is shown as sticks color-coded by atom type. Reducing and non-reducing ends of HA are labeled.

as follows: the first N-terminal  $\beta$ -sheet domain ( $\beta$ I-domain), a central  $\alpha$ -helical domain ( $\alpha$ -domain), and the second C-terminal  $\beta$ -sheet domain ( $\beta$ II-domain). The  $\alpha$ -domain is the primary catalytic domain and has an  $\alpha_5/\alpha_5$ -barrel structure (Fig. 1A). One end of this domain assumes the shape of a deep and elongated cleft, and it faces the  $\beta$ II-domain. The cleft is where the hyaluronan substrate, including the hexasaccharide, binds and where the catalytic residues are located (10).

The consecutive disaccharide building blocks of the HA hexasaccharide that bind in the cleft are termed HA1, HA2, and HA3 starting from the reducing end (Figs. 1, A and C, and 2A). The hexasaccharide hyaluronan substrate assumes a helical-like conformation with approximately a quarter of the turn accomplished by the three disaccharides of the current substrate. The individual sugar rings are in the expected chair conformation with the exception of the terminal sugar ring of the HA3 disaccharide that assumes a puckered structure resembling in part a distorted half-chair conformation. The tem-

perature factors for the substrate are relatively high which reflects significant mobility of the substrate in the cleft.

The substrate binds in the cleft formed by the opening in one end of the  $\alpha_5/\alpha_5$  barrel structure. The cleft has an elongated shape with dimensions similar to those of the native enzyme structure (1, 10). The major interactions between the hexasaccharide substrate and the amino acid residues of the cleft are listed in Table II and are shown in Fig. 2A. Specifically, the residues of the catalytic group, Asn<sup>429</sup>, His<sup>479</sup>, and Tyr<sup>488</sup>, take part in interactions with the chemical groups of the substrate as well as with other amino acid residues of the enzyme (Fig. 2, A and B) (10). The interactions of His<sup>479</sup> and Tyr<sup>488</sup> with the catalytically involved groups of the substrate are significantly longer than expected due to the widely open form of the cleft that likely is narrowed down during catalysis (see the enzyme flexibility section below). There are, however, no other residues present in close proximity to hyaluronan's either O4 glycosidic oxygen, C5 carbon, or the carboxyl group of the glucuronate (O6

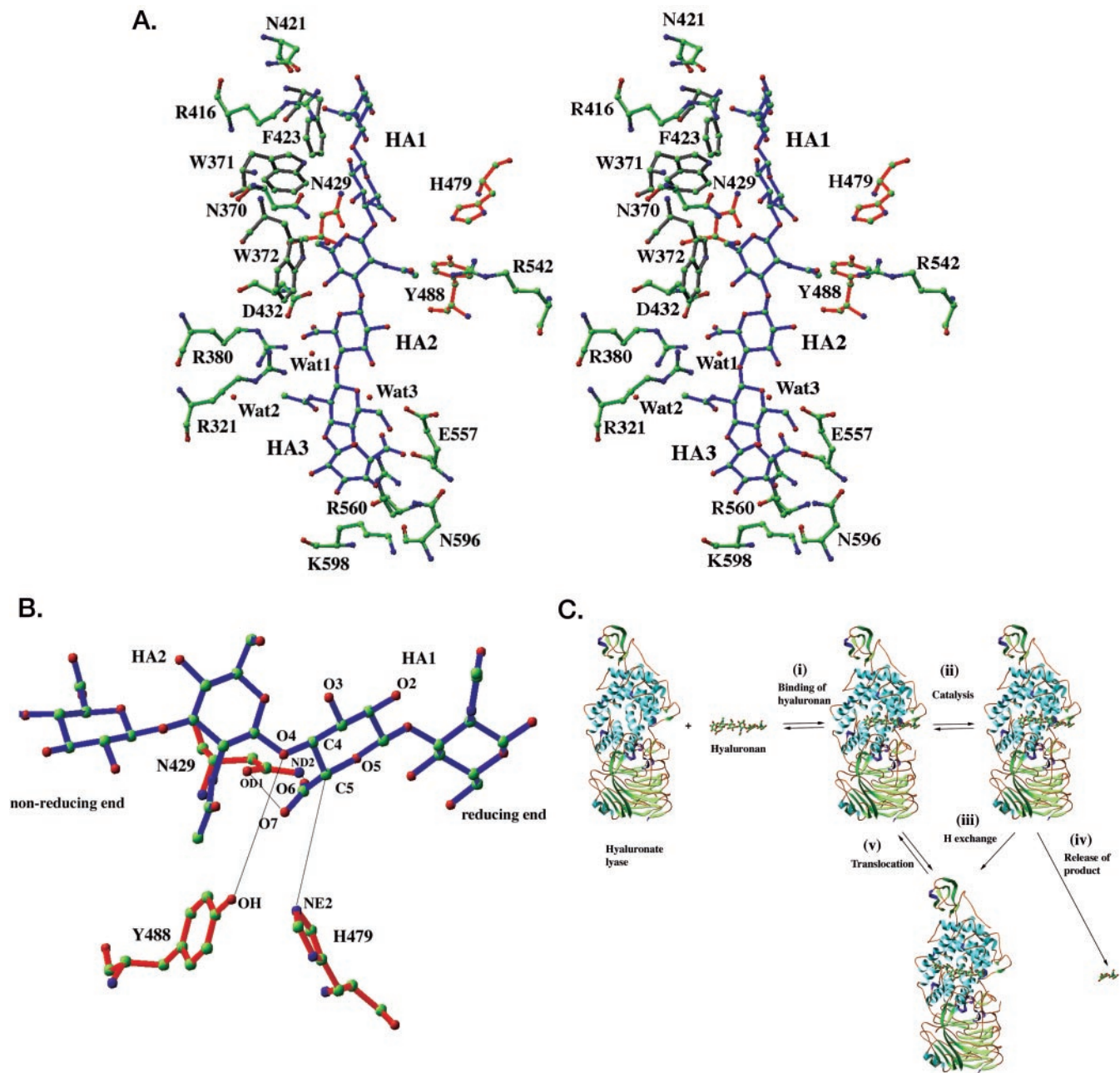


**FIG. 2. Enzyme-hyaluronan substrate interactions.** **A**, a stereo view of interactions in the structure of the complex. The hexasaccharide hyaluronan substrate molecule is shown in dark blue and selected protein amino acid residues are shown using standard color-coding for atom types. The substrate and selected residues are shown in a ball and stick fashion. The bonds of the catalytic residues are in red and the hydrophobic patch residue bonds are in gray. The spheres are depicted using standard color-codes for atoms. Three water molecules in the cleft are shown. HA1, HA2, and HA3 disaccharides are labeled. **B**, catalytic residues and the substrate. The hexasaccharide substrate chain (dark blue color for bonds) is shown with catalytic residues (red color for bonds) as follows: Asn<sup>429</sup>, His<sup>479</sup>, and Tyr<sup>488</sup>. Residues of the hydrophobic patch (Trp<sup>291</sup>, Trp<sup>292</sup>, and Phe<sup>343</sup>) and the negative patch (Glu<sup>388</sup>, Asp<sup>398</sup>, and Thr<sup>400</sup>) are not shown (see A). All atoms are color-coded by atom type. Interactions of the catalytic group residues and their targeted substrate atoms are shown by lines. The reducing and non-reducing ends of the substrate are labeled. Both ends of the substrate may extend in both directions to include longer polymeric hyaluronan chain. Selected atoms of the HA1 part of the substrate and the catalytic residues were labeled. The  $\beta$ 1,4-glycosidic linkage between HA1 and HA2 positions is to be cleaved. **C**, overall mechanism of hyaluronate lyase action. The steps for of the catalytic process are graphically shown using the ribbon drawing of the enzyme and a ball and stick rendition rendering of hyaluronan and their respective complexes. The major steps are as follows: (i) enzyme binding to the hyaluronan substrate, (ii) catalytic degradation of hyaluronan substrate resulting in polymeric hyaluronan and a disaccharide product, (iii) hydrogen exchange with microenvironment, (iv) disaccharide product release from the active site of the enzyme, and (v) translocation of the truncated hyaluronan substrate into the catalytic position.

and O7 oxygen atoms) of HA1 that could take part in the catalysis and substitute for any one of the three catalytic residues, Asn<sup>429</sup>, His<sup>479</sup>, and Tyr<sup>488</sup>. The three water molecules observed in the cleft, Wat<sup>1</sup>, Wat<sup>2</sup>, and Wat<sup>3</sup>, are not involved in catalysis as they are significantly separated from the catalytic residues, and they primarily interact only with the HA3 disac-

charide of the substrate (Fig. 2A and Table II). The residues of the negative patch located at the non-reducing end of the cleft, Glu<sup>468</sup>, Asp<sup>478</sup>, and Thr<sup>480</sup>, do not participate in any significant interactions with HA for the same reason as do the catalytic residues (widely open cleft). In addition, the hydrophobic patch residues located just next to the catalytic residues, Trp<sup>371</sup>,

TABLE II

Major interactions between hyaluronate lyase residues and the hexasaccharide hyaluronan substrate

The symbols assigned to the substrate atoms follow standard chemical nomenclature for sugar molecules (see Fig. 2B). Atoms were considered to be in the interacting distance if they were separated by 4.1 Å or less. For the catalytic residues Asn<sup>429</sup>, His<sup>479</sup>, and Tyr<sup>488</sup> even longer distances involving their target atoms in catalysis were also measured and reported.

Hexasaccharide/water atoms	Enzyme/water residues and atoms	Distance
NAc1 <sup>a</sup> of HA1		
C2	Å	
C3	Arg <sup>416</sup> NH1	2.98
O3	Arg <sup>416</sup> NH2	3.73
O6	Trp <sup>371</sup> NE1	3.68
O7	Phe <sup>423</sup> CG	3.97
O7	Arg <sup>416</sup> NH1	3.21
	Asn <sup>421</sup> OD1	3.80
GlcA1 of HA1		
C2	Trp <sup>371</sup> NE1	3.52
C5	His <sup>479</sup> NE2	5.68
O2	Trp <sup>371</sup> NE1	3.66
O3	Asn <sup>370</sup> OD1	3.89
O4 (glycosidic oxygen)	Tyr <sup>488</sup> OH	6.14
O6 (glucuronate CO <sub>2</sub> )	Asn <sup>429</sup> ND2	3.90
O7 (glucuronate CO <sub>2</sub> )	Asn <sup>429</sup> OD1	5.31
NAc2 of HA2		
C5	Trp <sup>372</sup> CD2	3.50
C6	Trp <sup>372</sup> CB	3.36
	Asn <sup>370</sup> ND2	3.32
C7	Tyr <sup>488</sup> OH	3.83
	Arg <sup>542</sup> NH2	3.81
C8	Tyr <sup>488</sup> OH	2.80
	Arg <sup>542</sup> NH2	3.89
O4	Trp <sup>372</sup> CZ3	3.54
O6	Asn <sup>370</sup> ND2	2.68
O7	Arg <sup>542</sup> NH2	3.00
	Asn <sup>660</sup> ND2	3.97
GlcA2 of HA2		
C4	Wat <sup>1</sup>	3.03
C6	Trp <sup>372</sup> CZ2	3.35
	Arg <sup>380</sup> NH2	3.52
O6 (glucuronate CO <sub>2</sub> )	Arg <sup>380</sup> NH1	2.80
	Trp <sup>372</sup> CZ2	3.45
	Asp <sup>432</sup> OD1	4.00
O7 (glucuronate CO <sub>2</sub> )	Arg <sup>321</sup> NH1	3.54
	Trp <sup>372</sup> CH2	2.93
	Arg <sup>380</sup> NH2	3.74
	Wat <sup>1</sup>	2.93
NAc3 of HA3		
C5	Arg <sup>380</sup> NH2	4.10
C8	Arg <sup>380</sup> NH1	3.05
	Wat <sup>2</sup>	3.72
O7	Wat <sup>3</sup>	3.87
GlcA3 of HA3		
C3	Lys <sup>598</sup> CB	3.49
C4	Asn <sup>596</sup> ND2	3.83
	Lys <sup>598</sup> CG	3.47
C5	Arg <sup>560</sup> NH2	3.72
C6	Arg <sup>560</sup> NH2	3.77
	Wat <sup>3</sup>	3.30
O3	Wat <sup>3</sup>	3.86
O4	Lys <sup>598</sup> CB	3.14
	Asn <sup>596</sup> ND2	3.09
O5	Arg <sup>560</sup> NH1	2.93
O6 (glucuronate CO <sub>2</sub> )	Lys <sup>598</sup> CG	3.45
	Wat <sup>3</sup>	3.81
O7 (glucuronate CO <sub>2</sub> )	Glu <sup>557</sup> OE2	3.28
	Arg <sup>560</sup> NH2	2.86
	Wat <sup>3</sup>	2.81
	Asn <sup>596</sup> ND2	3.53
	Arg <sup>560</sup> NH1	3.99

<sup>a</sup> GlcA1, GlcA2, and GlcA3 denote the β-D-glucuronic acid of HA1, HA2, and HA3 of hexasaccharide HA, whereas NAc1, NAc2, and NAc3 denote N-acetyl-β-D-glucosamine of HA1, HA2, and HA3, respectively.

Trp<sup>372</sup>, and Phe<sup>423</sup>, are involved in interactions predominantly with the hydrophobic ring structures of the HA1 and HA2 disaccharides of the substrate but not HA3 (Fig. 2A). These

interactions are likely responsible for the precise positioning of HA1 and HA2 disaccharides of hyaluronan for catalysis. Once this precise positioning is accomplished, all three catalytic residues are in the appropriate distances and in proper arrangement for the catalytic process to proceed forward (Fig. 2B).

### Flexibility Analyses

**Differences in Flexibility between *S. agalactiae* HL and *S. agalactiae* HL-βI**—A combined ED analysis of the CONCOORD ensembles of *S. agalactiae* HL (domains βI, α, and βII) and *S. agalactiae* HL-βI (domains α and βII) (Fig. 1B) reveals that the protein shows similar behavior in terms of the major collective fluctuations, both in the presence and absence of the βI domain (results not shown). This similarity is based on a comparison between the mean square fluctuation along the simulation for all the eigenvectors. The precise functionality of the βI domain has still not been fully determined and described (10). However, these results indicate that the presence of this domain does not affect the fluctuations in the other two domains of the protein (domain α and βII), suggesting that the βI domain is not directly involved in the main protein function, binding and degradation of hyaluronan substrate. These results agree with experimental observations, because protein activity remained essentially the same when this first domain was removed (14, 46, 47). This approach allows for the comparison of the two hyaluronate lyases from different streptococcal species without including the βI domain of *S. agalactiae* HL enzyme.

**Flexibility of the Enzyme in the Presence and Absence of the Hexasaccharide Substrate**—A combined ED analysis of CONCOORD simulations, with and without hexasaccharide substrate, showed that the main modes of collective fluctuation were remarkably similar and, therefore, were only moderately affected by the presence of the hyaluronan substrate. Interestingly, the third eigenvector (the collective mode of fluctuation with the third highest amplitude) describes a closure motion of the two domains (domains α and βII) similar to the difference observed between the previously reported *S. agalactiae* HL and *S. pneumoniae* HL x-ray structures (see Fig. 3). In summary, the protein is on average in a more closed configuration in the presence of the hyaluronan substrate, *i.e.* the protein structure apparently closes around the substrate.

***S. agalactiae* Hyaluronate Lyase Flexibility Analysis**—The largest amplitude modes of the collective fluctuation of the protein, as described by the first three eigenvectors of the ED analysis of the ensemble of CONCOORD structures, are illustrated in Figs. 4–6. All three main motions detected are likely related to the protein function in a different manner. Fig. 4A illustrates the two extreme structures of *S. agalactiae* HL along eigenvector 1 (in all figures, for clarity of the presentation, the βI domain of *S. agalactiae* HL structure is not shown because it does not affect the main modes of molecular motion (see above)). The motion described by the eigenvector 1 can be illustrated as a rotation/twist of the catalytic α-domain relative to the C-terminal βII-domain (Fig. 4B).

The second largest collective fluctuation, described by eigenvector 2, is illustrated in Fig. 5, A and B, which shows the two extreme structures along this mode of flexibility. The movement can be described as a closure motion that affects the active site cleft such that when the entrance to the cleft opens, the exit closes, and vice versa (Fig. 5C). The overall electrostatic potential of the protein is affected by this motion, and its putative effects are discussed below (Fig. 5A).

Finally, the enzyme motion described by eigenvector 3 consists of an opening/closing of the access to the substrate-bind cleft, which exposes residues from the active site and from

the hydrophobic patch to the bound hyaluronan substrate (Fig. 6, A and C). The molecular surface of the enzyme, colored by its curvature, is illustrated in Fig. 6B showing the cleft in the more open state.

**Comparison of the Flexibility between the *S. agalactiae* and *S. pneumoniae* Hyaluronate Lyases**—In this section the flexibility of two hyaluronate lyases from different streptococcal species is compared. As the *S. pneumoniae* HL structure represents the hyaluronate lyase enzyme without the  $\beta$ I domain, and because the  $\beta$ I domain was found to have a negligible effect on the main domain fluctuations in *S. agalactiae* HL (see above), the  $\beta$ I domain of the *S. agalactiae* HL enzyme was left out of further analyses (Fig. 1B).

The flexibility studies showed no significant differences in the enzyme fluctuation between the *S. agalactiae* HL and *S. pneumoniae* HL structures, which indicates similar large concerted motions of their common structural core (results not shown). These results are in agreement with biochemical and structural data suggesting that the *S. pneumoniae* HL and *S. agalactiae* HL enzymes act in a very similar way (10, 14, 46, 47). Both enzymes have similar three-dimensional structure, and both degrade the substrate to disaccharide units of hyaluronan as the end product with similar specific activities (14, 47). This behavior, in which two proteins with a similar structure and that share a similar flexibility, is also characteristic of other enzymes. The comparison of similar GTPase domains of  $G\alpha_t$ -GDP and p21<sup>ras</sup> similarly found common dynamic properties for their equivalent domains (48). Because the modes of fluctuation for the two proteins were found to be fairly similar, the functional implications of the simulations of hyaluronate lyase enzymes were analyzed using primarily the data for the *S. agalactiae* HL enzyme.

### Functional Implications

Structural and dynamic characteristics of the hyaluronate lyase enzymes from streptococcal species were analyzed, in conjunction with our previous work describing the flexibility of the *S. pneumoniae* enzyme (23), to attempt a better understanding of the molecular basis of their function. The analysis was primarily focused on elucidating the mechanisms responsible for the processive degradation of the substrate.

The proposed catalytic process for both the *S. agalactiae* and *S. pneumoniae* hyaluronate lyase enzymes has been proposed, analyzed, and described previously (1, 10, 13, 23). Briefly, the process consists of five general steps (Fig. 2C) as follows. (i) Binding of the enzyme utilizes its largely positive cleft to the negatively charged hyaluronan substrate and the precise relative positioning of HA and the enzyme by the hydrophobic patch residues Trp<sup>371</sup>, Trp<sup>372</sup>, and Phe<sup>423</sup> interacting with hydrophobic sugar rings of HA (Fig. 2A and Table II). (ii) The catalysis, performed by the catalytic residues Asn<sup>429</sup>, His<sup>479</sup>, and Tyr<sup>488</sup>, results in breaking of the glycosidic bond, transfer of one hydrogen from HA, C5 hydrogen, to His<sup>479</sup> NE2 of the enzyme, and one from the enzyme, Tyr<sup>488</sup> OH, to the glycosidic oxygen O4 of HA (Fig. 2B). (iii) The exchange of hydrogens with the water microenvironment in the cleft makes the enzyme chemically ready for the next round of catalysis. (iv) The consecutive release of the generated disaccharide product from the cleft uses the electrostatic repulsion of the negative product from the residues of the negative patch Glu<sup>468</sup>, Asp<sup>478</sup>, and Thr<sup>480</sup> (Fig. 1C). (v) This final step is the translocation of the remaining truncated HA substrate in the cleft by one disaccharide unit in the direction of the reducing end of HA (Fig. 2C). The initial binding of HA to the enzyme is likely random with the endolytic cleavage of HA followed by the exolytic processive cleavage of one disaccharide unit at the time until the remaining

whole HA chain is fully degraded (10, 11, 23). The substrate remains bound to the enzyme during the whole process of degradation. Some details of the processivity are described elsewhere (23) and are described in more detail below. The catalytic step ii of the five-step process described above is a complex progression which in turn also involves several substeps as described: (a) Asn<sup>429</sup> interactions with the carboxyl group of the glucuronate of HA1 disaccharide leading to the acidification of the C5 hydrogen; (b) withdrawal of this hydrogen by His<sup>479</sup> followed by rehybridization of the C5 carbon to  $sp^2$ ; (c) donation of the hydrogen by Tyr<sup>488</sup> OH to the glycosidic oxygen, O4, causing rehybridization of the C4 carbon to  $sp^2$  and the simultaneous formation of the C4–C5 double bond (Fig. 2B) (1, 10, 23).

### Enzyme Flexibility and the Processivity Mechanism of Hyaluronan Degradation

The individual modes of collective enzymatic fluctuation are likely involved in the processive mechanism of hyaluronan degradation of the enzyme. Although the ED technique yields individual collective motions, all the modes interplay with each other in a complex manner, and therefore, not necessarily all individual modes will correspond to a specific functional task. However, for clarity, putative functional aspects of the dominant modes will be discussed based on the individual modes of flexibility. The  $\alpha$ -domain containing the positive patch is responsible for the majority of protein-ligand contacts. The twist motion described by eigenvector 1 produces exposure of the positively charged cleft (positive patch) to the environment of the enzyme and the substrate (Fig. 4). Hence a twisting motion of the  $\alpha$ -domain relative to the  $\beta$ II-domain (described by eigenvector 1), with the cleaved substrate bound to the former ( $\alpha$ -domain), likely facilitates the shift of the ligand along the cleft in order to reposition it in the catalytic site and ready for further cleavage. Comparison of the minimum and the maximum projection structures of eigenvector 1 showed that the distances between the hydrophobic residues in the two extreme structures (11.6, 11.1, and 12.5 Å for Trp<sup>371</sup>, Trp<sup>372</sup>, and Phe<sup>423</sup>, respectively) match closely the distance between two disaccharide units of around 10.6 Å. Thus, the twist/rotation of the  $\alpha$ -domain likely allows these residues to shift by a distance equivalent to 2 units of the ligand and to grip the substrate in order to shift it in the cleft by two disaccharides in the reducing end direction for further catalysis of the degradation of the polymeric substrate.

Another movement involving the two domains (described by eigenvector 2) shows that when the structure of the enzyme attains the conformation of the extreme difference from the crystal structure, two distinct factors were found to contribute to a change in the electrostatic characteristics favorable for the binding of the negatively charged ligand. First, the positive patch on the  $\alpha$ -domain becomes more exposed, in particular residues Arg<sup>321</sup>, Arg<sup>322</sup>, Arg<sup>435</sup>, and Arg<sup>380</sup>. Residues from the active site, the hydrophobic and the negative patches remain inaccessible and are not influenced by this motion. Second, in this motion the overall reduction of the negative electric field is observed around the C-terminal  $\beta$ II-domain (Fig. 5).

The opening/closing of the access to the substrate binding cleft (as described by eigenvector 3) brings a catalytic histidine residue closer to the hyaluronan substrate  $\beta$ 1,4-glycosidic bond (Fig. 6). Moreover, the structures described by this third eigenvector strongly overlap with the differences reflected by the structural difference between the x-ray crystal structures of *S. agalactiae* HL and *S. pneumoniae* HL (Figs. 3 and 6). This analysis clearly indicates that the difference observed between the x-ray structures of the *S. agalactiae* HL and *S. pneumoniae* HL hyaluronate lyase enzymes

**FIG. 3. DynDom analysis of the difference between the *S. pneumoniae* and *S. agalactiae* hyaluronate lyase x-ray crystal structures.** Shown is the x-ray structure of *S. agalactiae* HL, with the yellow arrow depicting the rotation axis for the domain transition toward the *S. pneumoniae* HL structure, in which the red domain rotates with respect to the blue domain. The domain motion corresponds to a closure motion (white arrows). The green residues provide the flexible linker between the two domains.

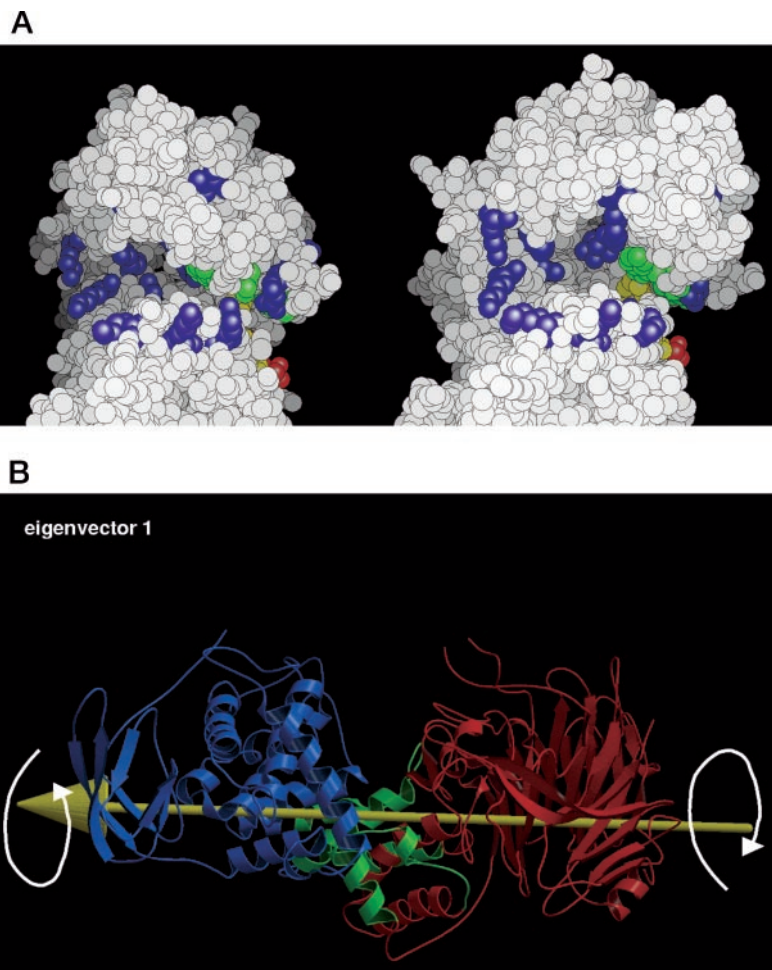
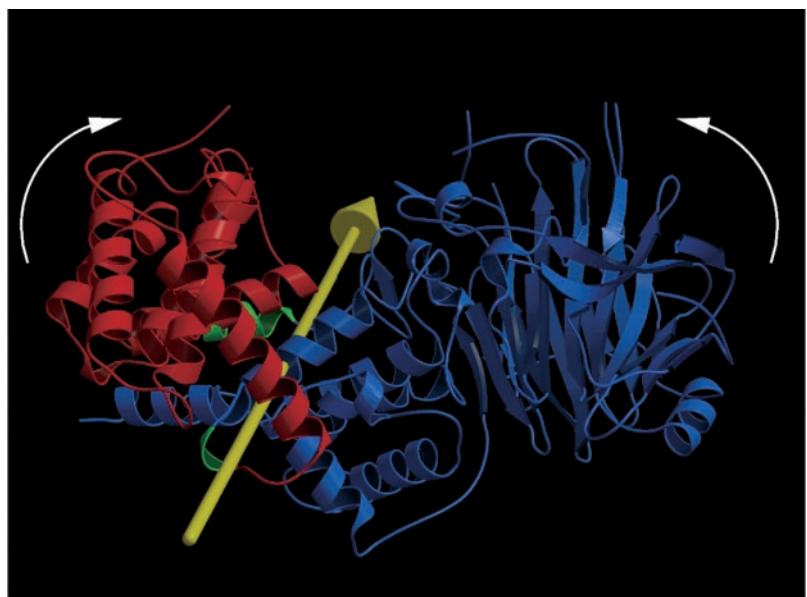


**FIG. 4. Essential dynamics analysis of CONCOORD simulation for eigenvector 1.** **A**, atomic representation of the minimum (left) and the maximum (right) projection structures derived from the ED analysis. Residues from 224 to 234 are the main ones involved in the twist of the  $\alpha$ -domain, allowing a better exposition of the residues from the positive patch (residues in blue). Residues from the hydrophobic and the negative patches and from the catalytic site are essentially static in the mode of action described by this eigenvector, and are colored in green, red and yellow, respectively. **B**, DynDom analysis of the two extreme structures along the first eigenvector. This mode describes a twisting motion of the two domains with respect to each other. As in Fig. 3, the yellow arrow corresponds to the rotation axis for the domain motion of the red domain with respect to the blue domain, with the intermediate (linker) regions colored green.

corresponds to the conformational change that is accessible to both proteins as one of the major collective fluctuations. The different crystallization conditions for these two enzymes contributed to the selection of the different structures in these different crystals (14, 47). The amplitude of the fluctuation in the simulations also is comparable with the magnitude of the difference between the experimental structures observed: the simulations performed started from the (open

structure) *S. agalactiae* HL structure and ended with the closed structure as in the *S. pneumoniae* HL structure (closed structure).

#### Structural Aspects Related to the Mechanism of Processivity

The comparison between the *S. agalactiae* and *S. pneumoniae* hyaluronate lyase enzyme structures showed that the

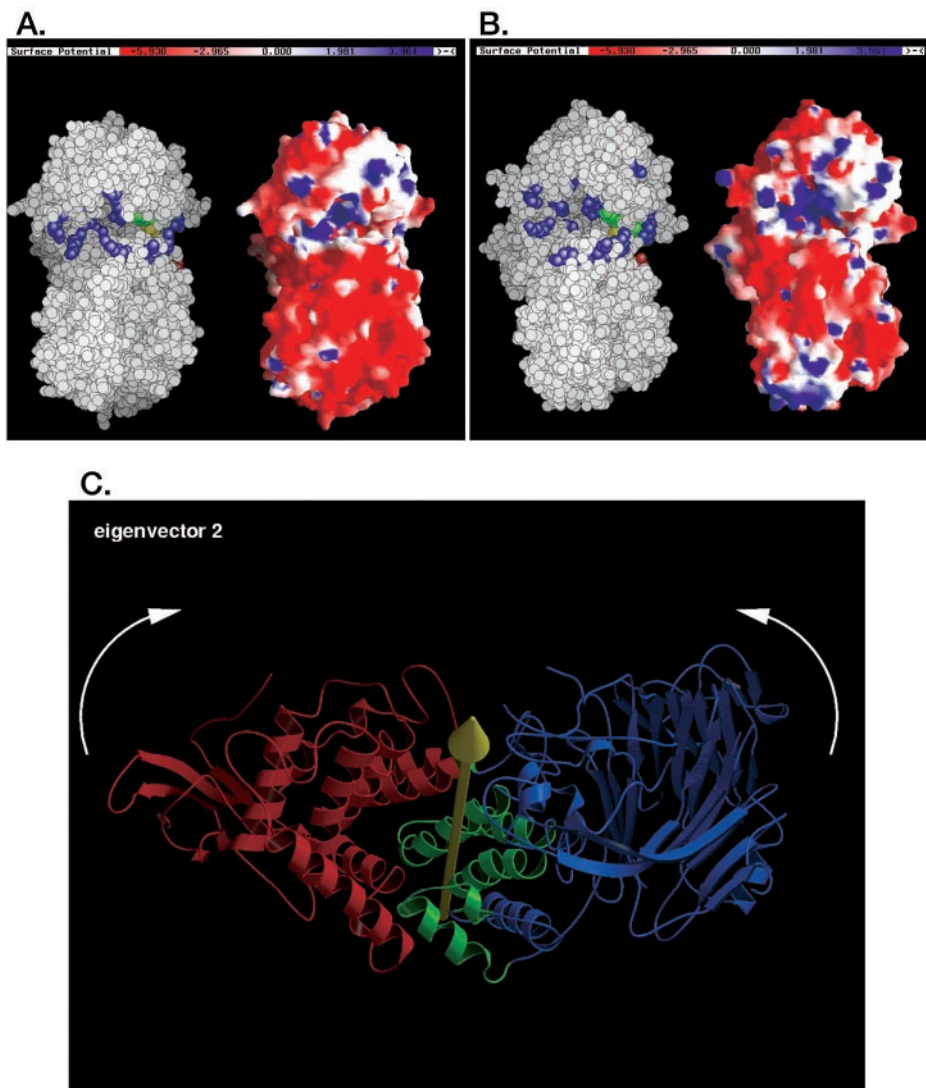


**FIG. 5. Essential dynamics analysis of CONCOORD simulation for eigenvector 2.** The atomic representations of the minimum (A) and the maximum (B) projection structures. The structures show the larger number of residues from the positive patch in consequence of the  $\alpha$ -domain rotation described by the eigenvector 2 mode of action. The solvent-accessible surfaces are shown on the right with positive and negative electrostatic potential colored blue and red, respectively. The units of the scale are  $kT$  where  $k$  is the Boltzmann constant and  $T$  is temperature. The catalytic site cleft is shown in the center of the  $\alpha$ -domain. The increase of the blue area is due to the exposure of a larger number of the positive patch residues in the maximum projection structure from the essential dynamic analysis. The small electrostatically negative area at the half-bottom of the figure ( $\beta$ II-domain) is caused by the domain rotation in this motion. C, DynDom analysis of the two extreme structures along the second eigenvector. This mode describes a closure motion that affects the active site cleft such that when the entrance opens, the exit closes, and vice versa, and as such might be involved in substrate uptake and/or release. As in Fig. 3, the yellow arrow corresponds to the rotation axis for the domain motion of the red domain with respect to the blue domain, with the intermediate (linker) regions colored green.

cleft of the *S. agalactiae* enzyme is significantly wider than that of *S. pneumoniae* hyaluronate lyase (1, 9, 10, 13). The narrowest part of the cleft width exceeds that of the *S. pneumoniae* HL by nearly 7 Å (10). Because the sequence identity between *S. pneumoniae* HL and *S. agalactiae* HL is 54.5%, and their structures show a high degree of similarity, a structural comparison was made in terms of dynamic domains, using the DynDom program. Fig. 3 shows the results of this analysis based on the *S. agalactiae* HL (10) and *S. pneumoniae* HL crystal structures (1). The difference between both structures corresponds to a clear domain motion (Fig. 3, white arrows) in which the  $\alpha$ - and  $\beta$ II-domains come closer with respect to each other to close up the cleft (the *S. agalactiae* HL structure is more open (“open structure”) than is the *S. pneumoniae* HL structure (“closed structure”)), burying the active site cleft between them. The yellow arrow in Fig. 3 corresponds to the rotation axis corresponding to the domain motion. A rotation axis perpendicular to the axis connecting the two domains, as is the case here, indicates a pure closure motion. The residues near the rotation axis (colored in green) can be considered hinge regions for this motion (Fig. 3). The hinge regions involve residues 94–98 and 283–288 of the enzyme. Gly<sup>95</sup>, in particular, seems to play a critical role as a hinge region residue. The widening and closing of the access to the cleft as described by eigenvector 3 allows for more movement of the substrate already bound in the cleft and also affects the flexibility of the

cleft as well as the whole enzyme. This flexibility is necessary as the cleft needs to close down to bring all catalytic residues into the positions appropriate for the catalytic process to take place (9, 10, 23). Such flexibility was already observed for the *S. pneumoniae* hyaluronate lyase (23), and therefore, it is not unexpected that the *S. agalactiae* enzyme has similar properties in this respect. The resulting relatively weaker binding of the substrate to the flexible enzyme, compared to one with a rigid structure, might be relevant physiologically. As the enzyme degrades hyaluronan in a processive mode of action, a weaker binding of substrate might allow for easier shifting of the enzyme with respect to the substrate (sliding/threading mechanism of processivity) along the cleft length (11, 23). For the processivity to take place, the substrate binding needs to be relatively weak in order to allow for the sliding of the enzyme along the substrate toward its non-reducing end to bring the catalytic part of the cleft over the  $\beta$ 1,4-glycosidic linkage to be cleaved (23, 48).

#### Selection of the $\beta$ 1,4-Glycosidic Bond for Catalysis

The structure of the complex of the hexasaccharide hyaluronan substrate with the *S. agalactiae* hyaluronate lyase was also utilized to elucidate the mechanism of the enzyme selection of only the  $\beta$ 1,4 bonds of the substrate for cleavage but not the  $\beta$ 1,3 bonds. Several factors appear to contribute to this

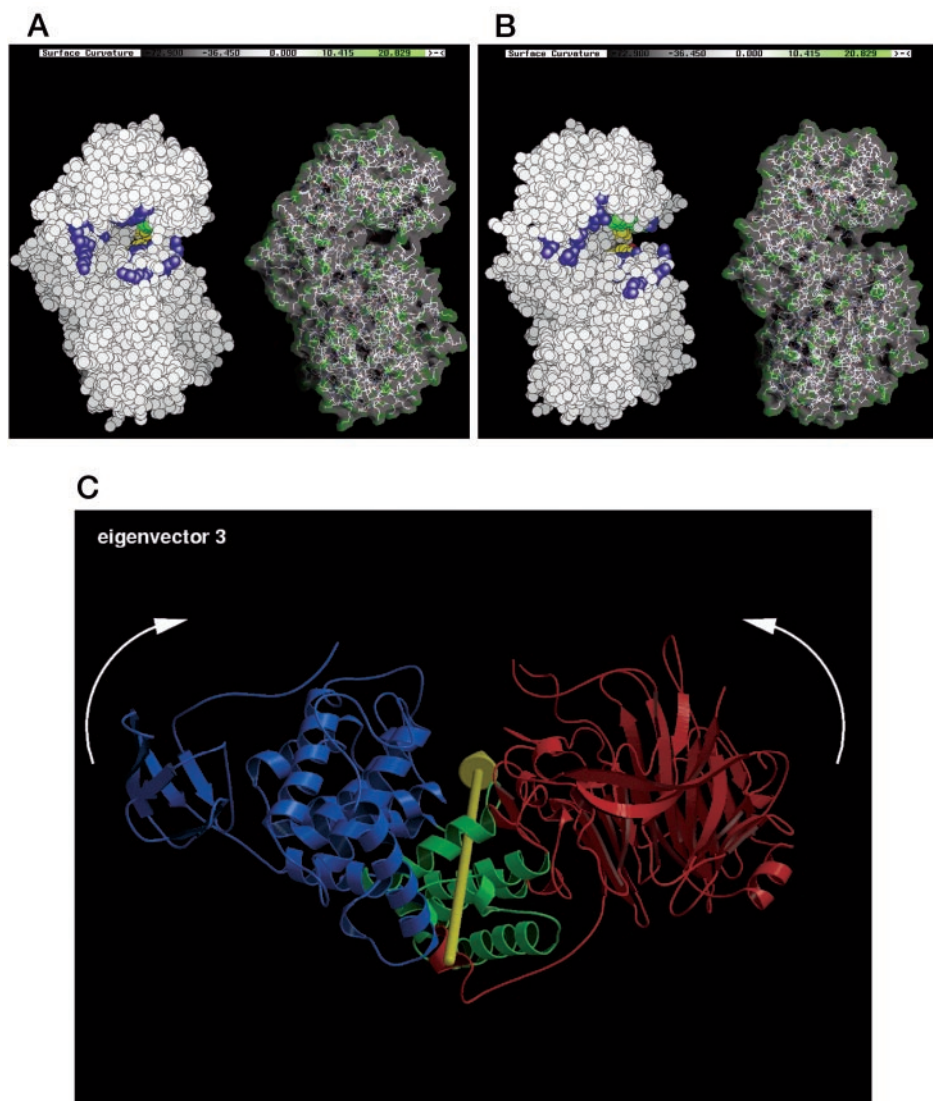


**FIG. 6. Essential dynamics analysis of CONCOORD simulation for eigenvector 3.** The atomic representations of the minimum (A) and the maximum (B) projection structures of eigenvector 3. The structures show the exposure of the residues from the active site (in yellow) and from the hydrophobic patch (in green). Residues from the positive and negative patches are colored in blue and red, respectively. The surface is color-coded on the right by curvature with green being used for convex surface and gray for concave surface. Note that the cleft of the maximum projection is more open than for the minimum projection allowing a better ligand accessibility to the binding pocket. C, DynDom analysis of the two extreme structures along the third eigenvector. This mode describes a closure motion of the two domains, opening and closing the active site cleft. This mode of motion shows a high degree of overlap with the difference vector derived from the x-ray structures of *S. pneumoniae* HL and *S. agalactiae* HL (see Figs. 1B and 3). As in Fig. 3, the yellow arrow corresponds to the rotation axis for the domain motion of the red domain with respect to the blue domain, with the intermediate (linker) regions colored green.

selection process. First, as indicated in Table II, *N*-acetyl- $\beta$ -D-glucosamine of HA2 disaccharide (NAc2) of the bound substrate makes two hydrogen bonds with the enzyme residues. These bonds involve interactions between the oxygen of the NAc2 amide group and Arg<sup>542</sup> and between the 6-hydroxyl group and Asn<sup>370</sup>. The different chemical nature of the  $\beta$ -D-glucuronic acid (GlcA), another sugar building block of hyaluronan, indicates that the similar hydrogen bonds as those formed with the NAc2 could not form if the GlcA disaccharide were placed at the same site as is NAc2. By using rudimentary modeling based on the structure of the complex, when the enzyme-bound substrate is shifted along the cleft to place the  $\beta$ 1,3 bond close to the catalytic residues, further obstacles such as steric clashes between the substrate and the enzyme are evident. The most significant of these clashes involves the carboxyl group of the GlcA moiety and Trp<sup>372</sup> (distance of 1.65 Å). In addition, no charge compensation is available for the carboxylate group of the GlcA disaccharide; indeed, the closest residue to this carboxylate is negatively charged Asp<sup>373</sup>. Based on modeling, the position of the substrate can be adjusted to minimize the steric clashes, but by doing so the  $\beta$ 1,3 bond is removed from the position suitable for catalysis. Therefore, in both possible cases described above the cleavage of the  $\beta$ 1,3-glycosidic bond is not possible by the hyaluronate lyase. The geometry of both the hyaluronan substrate and the cleft of the

enzyme is responsible for the selection of only the  $\beta$ 1,4-glycosidic bond for degradation by the enzyme.

### Conclusions

The mechanism of degradation of hyaluronan was investigated for a long time by biochemical methods (*e.g.* Refs. 49 and 50). However, the more recent structural studies allowed for the precise determination and analysis of this mechanism. These structural studies allowed for the identification of the specific residues involved in the catalysis and the assignment of their role in this process (1, 9, 10, 13, 23). In addition, studies of other polysaccharide-degrading enzymes that utilize the  $\beta$ -elimination process were investigated. These studies include structure determination of *Flavobacterium heparinum* chondroitin AC lyase (51) and *Sphingomonas* species Alginate lyase A1-III (52). In general, the mechanisms of action proposed for *F. heparinum* chondroitin AC lyase and *Sphingomonas* species alginate lyase A1-III are similar to that proposed for the *S. agalactiae* and *S. pneumoniae* hyaluronate lyases (9, 13). The details as to the precise identification of which residues are involved in such catalysis and their role (*i.e.* the acid and base required for catalysis corresponding to His<sup>479</sup> and Tyr<sup>488</sup> for the *S. agalactiae* hyaluronate lyase) are still not clear. However, the structural differences present between these enzymes and hyaluronate lyase might very well account for such differences.

For the first time in this work, the dynamic aspects facilitating the processive nature of hyaluronate lyase were described. The results showed a combination of dynamic and structural features related to substrate binding, catalysis, processivity, and product release. These results may well be relevant to and explain properties of other proteins, including numerous polysaccharide-degrading enzymes, utilizing the processive mode of action in their catalysis.

**Acknowledgments**—Diffraction data for this study were collected at Brookhaven National Laboratory, National Synchrotron Light Source x25 beamline, or at Advanced Photon Source, Structural Biology Center at the beamline 19-BM, Argonne National Laboratory. We thank the staff of these facilities for their help and assistance with diffraction data collection.

## REFERENCES

- Li, S., Kelly, S. J., Lamani, E., Ferraroni, M., and Jedrzejas, M. J. (2000) *EMBO J.* **19**, 1228–1240
- Musser, J. M., Mattingly, S. J., Quentin, R. T., Goudeau, A., and Selander, P. K. (1989) *Proc. Natl. Acad. Sci. U.S.A.* **86**, 4731–4735
- Rolland, K., Marois, C., Siquier, V., Cattier, B., and Quentin, R. (1999) *J. Clin. Microbiol.* **37**, 1892–1898
- Laurent, T. C., and Fraser, R. E. (1992) *FASEB J.* **6**, 2397–2404
- McCourt, P. A. G. (1999) *Matrix Biol.* **18**, 427–432
- Toole, B. P., Goldberg, R. L., Chi-Rosso, G., Underhill, C. B., and Orkin, R. W. (1984) in *The Role of Extracellular Matrix in Development* (Trelstad, R. C., ed) pp. 43–66, Alan R. Liss, Inc., New York
- Courtiss, E. H., Ransil, B. J., and Russo, J. (1995) *Plast. Reconstr. Surg.* **95**, 876–883
- Menzel, E. J., and Farr, C. (1998) *Cancer Lett.* **131**, 3–11
- Jedrzejas, M. J. (2000) *Crit. Rev. Biochem. Mol. Biol.* **35**, 221–251
- Li, S., and Jedrzejas, M. J. (2001) *J. Biol. Chem.* **276**, 41407–41416
- Baker J. R., and Pritchard, D. G. (2000) *Biochem. J.* **348**, 465–471
- Pritchard, D. G., Trent, J. O., Li, X., Zhang, P., Egan, M. L., and Baker, J. R. (2000) *Proteins Struct. Funct. Genet.* **40**, 126–134
- Jedrzejas, M. J. (2001) *Microbiol. Mol. Biol. Rev.* **65**, 187–207
- Jedrzejas, M. J., and Chantalat, L. (2000) *Acta Crystallogr. Sect. D Biol. Crystallogr.* **56**, 460–463
- Gase, K., Ozegowski, J., and Malke, H. (1998) *Biochim. Biophys. Acta* **1398**, 86–98
- Lin, B., Hollingshead, S. K., Coligan, J. E., Egan, M. L., Baker, J. R., and Prichard, D. G. (1994) *J. Biol. Chem.* **269**, 30113–30116
- Kelly, S. J., Taylor, K. B., Li, S., and Jedrzejas, M. J. (2001) *Glycobiology* **11**, 297–304
- Otwinowski, Z., and Minor, W. (1997) *Methods Enzymol.* **276**, 307–326
- Brunger, A. T., and Warren, G. L. (1998) *Acta Crystallogr. Sect. D Biol. Crystallogr.* **54**, 905–921
- Brunger, A. T. (1992) *Nature* **355**, 472–474
- Jones, T. A., Zhou, J. Y., Cowan, S. W., and Kjeldgaard, M. (1991) *Acta Crystallogr. Sect. A* **47**, 110–119
- Rice, L. M., and Brunger, A. T. (1994) *Proteins Struct. Funct. Genet.* **19**, 277–290
- Jedrzejas, M. J., Mello, L. V., de Groot, B. L., and Li, S. (2002) *J. Biol. Chem.* **277**, 28287–28297
- Ponnuraj, K., and Jedrzejas, M. J. (2000) *J. Mol. Biol.* **299**, 885–895
- Laskowski, R. A., MacArthur, M. W., Moss, D. S., and Thornton, J. M. (1993) *J. Appl. Crystallogr.* **26**, 283–291
- Kleywegt, G. J., and Jones, T. A. (1996) *Acta Crystallogr. Sect. D Biol. Crystallogr.* **52**, 829–832
- Hayward, S., Kitao, A., and Berendsen, H. J. C. (1997) *Proteins Struct. Funct. Genet.* **27**, 425–437
- Hayward, S., and Berendsen, H. J. C. (1998) *Proteins Struct. Funct. Genet.* **30**, 144–154
- Vriend, G. (1990) *J. Mol. Graphics* **8**, 52–56
- De Groot, B. L., van Aalten, D. M., Scheek, R. M., Amadei, A., Vriend, G., and Berendsen, H. J. C. (1997) *Proteins Struct. Funct. Genet.* **29**, 240–251
- De Groot, B. L., Vriend, G., and Berendsen, H. J. C. (1999) *J. Mol. Biol.* **286**, 1241–1249
- Kleinjung, J., Bayley, P., and Fraternali, F. (2000) *FEBS Lett.* **470**, 257–262
- Labrou, N. E., Mello, L. V., and Clonis, Y. D. (2001) *Biochem. J.* **358**, 101–110
- Amadei, A., Linssen, A. B., and Berendsen, H. J. C. (1993) *Proteins Struct. Funct. Genet.* **17**, 412–425
- Van Aalten, D. M. F., Findlay, J. B. C., Amadei, A., and Berendsen, H. J. C. (1995) *Protein Eng.* **8**, 1129–1135
- Van Aalten, D. M. F., Jones, P. C., Sousa, M., and Findlay, J. B. C. (1997) *Protein Eng.* **10**, 31–37
- Schappach, A., and Holtje, H. D. (2001) *Pharmazie* **56**, 435–442
- Lindahl, E., Hess, B., and van der Spoel, D. (2001) *J. Mol. Model.* **7**, 306–317
- Carson, M. (1997) *Methods Enzymol.* **277**, 493–505
- Nicholls, A., Sharp, K. A., and Honig, B. (1991) *Proteins Struct. Funct. Genet.* **11**, 281–296
- Kraulis, P. J. (1991) *J. Appl. Crystallogr.* **24**, 946–950
- Esnouf, R. M. (1997) *J. Mol. Graph. Model.* **15**, 132–134, 112–113
- Merritt, E. A., and Bacon, D. J. (1997) *Methods Enzymol.* **277**, 505–524
- Park, Y., Cho, S., and Linhardt, R. J. (1997) *Biochim. Biophys. Acta* **1337**, 217–226
- Shimada, E., and Matsumura, G. (1980) *J. Biochem. (Tokyo)* **88**, 1015–1023
- Jedrzejas, M. J., Chantalat, L., and Mewbourne, R. B. (1998) *J. Struct. Biol.* **121**, 73–75
- Jedrzejas, M. J., Mewbourne, R. B., Chantalat, L., and McPherson, D. T. (1998) *Protein Expression Purif.* **13**, 83–89
- Breyer, W. A., and Matthews, B. W. (2001) *Protein Sci.* **10**, 1699–1711
- Gacesa, P. (1987) *FEBS Lett.* **212**, 199–202
- Greiling, H., Stuhlsatz, H. W., Eberhard, T., and Eberhard, A. (1975) *Connect. Tissue Res.* **3**, 135–139
- Huang, W., Boju, L., Tkalec, L., Su, H., Yang, H. O., Gunay, N. S., Linhardt, R. J., Kim, Y. S., Matte, A., and Cygler, M. (2001) *Biochemistry* **40**, 2359–2372
- Yoon, H. J., Hashimoto, W., Miyake, O., Murata, K., and Mikami, B. (2001) *J. Mol. Biol.* **307**, 9–16
- Brunger, A. T., and Kruckowski, A. (1990) *Acta Crystallogr. Sect. A* **46**, 585–593